

# High temperature characterization of piezoelectric lithium niobate using electrochemical impedance spectroscopy resonance method

Hector de Castilla,<sup>1</sup> Pierre Bélanger,<sup>1</sup> and Ricardo J. Zednik <sup>1</sup>

<sup>1</sup> *Department of Mechanical Engineering, École de Technologie Supérieure,  
Université du Québec, Montréal (Québec), H3C1K3, Canada*

## Abstract

Piezoelectric materials reversibly deform when exposed to an electric field. This property is indispensable to modern engineering devices, enabling a wide range of sensors and actuators. However, unfortunately conventional piezoelectric materials are limited to operating temperatures of below approximately 200 °C. Lithium niobate is a promising candidate for high temperature applications (above 500 °C), as it has a high Curie temperature (1200 °C) and good piezoelectric properties. Nevertheless, degradation mechanisms occurring at elevated temperatures are not fully understood, although they are known to interfere with the piezoelectric behavior. In addition, the material properties of this technologically promising ceramic have not been adequately characterized at high temperatures, particularly when excited at high frequencies, due to the difficulty of performing such measurements. We therefore employ an electrochemical impedance spectroscopy resonance method using a novel analytical model to determine the material properties of single crystal lithium niobate over the wide frequency range of 100 kHz to 7 MHz for temperatures up to 750 °C. We find that lithium niobate retains its good piezoelectric properties over this entire frequency and temperature range, and rule out suspected degradation mechanisms involving ionic conductivity or vacancy diffusion.

## 1. Introduction

Piezoelectric materials are well-known to have important applications in sensors, actuators, MEMS, and energy harvesting [1–3]. There is growing interest in using this exciting class of materials at high temperatures and in harsh environments, such as for structural health monitoring of hot components in combustion engines, nuclear power plants, and petroleum refineries. Unfortunately, conventional piezoelectric materials begin to deteriorate above about 200 °C [4]. Alternative materials that are piezoelectric up to higher temperatures tend to suffer from poor performance, including small piezoelectric coefficients, electromechanical coupling factors, or limited Curie temperatures [5].

However, a promising candidate is the ceramic lithium niobate ( $\text{LiNbO}_3$ ): its Curie temperature is around  $1200^\circ\text{C}$  and one study claims good quasi-static piezoelectric properties between  $600^\circ\text{C}$  and  $1000^\circ\text{C}$  [6] for at least seven hours. In addition, this material appears to retain reasonable electromechanical properties over this temperature range [7], at least over short time periods. Nevertheless, the literature discusses numerous electro-chemical deterioration mechanisms that degrade lithium niobate's piezoelectric properties at these temperatures [8–11]. This uncertainty stems from the technical challenge of measuring piezoelectric properties and underlying mechanisms at high temperatures. We therefore leverage an electrochemical impedance spectroscopy resonance method with a new analytical model to characterize lithium niobate at high temperatures and frequencies to help resolve this uncertainty.

## 2. Method

The resonance method requires an explicit model to describe the electrochemical impedance spectrum as a function of the intrinsic properties of the material, the geometry, and the density [12]. The electrochemical impedance spectrum of a material not only captures the motion of free electrons, but also includes the contribution of other charge carriers, such as ionic and vacancy displacement. In order to reduce the degrees of freedom, an accurate measurement of the geometry and the density is necessary [13,14]. Then, the intrinsic properties of the material can be extracted by performing a regression analysis of the measured data to the explicit model. This means that the elasticity, the piezoelectric coefficients, and the permittivity can be extracted from an electrochemical impedance spectrum [15]. The challenge of using this method is selecting an appropriate explicit model. In this article, we employ a three dimensional analytical model based on first principles [16]. This model is a generalization of Brissaud's work [17,18], and predicts most resonances and their harmonics, including shear modes and coupled modes. Thus, the sample does not need to have a specific aspect ratio [19], and almost all the intrinsic properties can be deduced. This model assumes that the displacement field inside the piezoelectric material is a linear superposition of the nine phonon waves, as in Equations (1) and (2), defined by the Christoffel equations along the three axes of the rectangular cuboid sample.

$$U(x,y,z,t) = \sum_{i=1}^3 (A_{x,i} \cdot V_{x,i} \cdot \sin(\alpha_{x,i} \cdot x) + A_{y,i} \cdot V_{y,i} \cdot \sin(\alpha_{y,i} \cdot y) + A_{z,i} \cdot V_{z,i} \cdot \sin(\alpha_{z,i} \cdot z)) \cdot e^{j\omega t} \quad (1)$$

$$\alpha_{x,i} = \frac{\omega}{v_{x,i}} \quad (2)$$

$V_{x,i}$  is the first eigenvector of the Christoffel equation for the x direction,  $v_{x,i}$  is the associated velocity,  $\omega$  is the pulsation, and  $A_{x,i}$  is the undetermined constant required by the linear superposition assumption. The strain field is easily deduced from this displacement field. Finally, the piezoelectric Equations (3) are solved for the boundary conditions:

$$\begin{cases} T = c_E \cdot S - e^t \cdot E \\ D = e \cdot S + \epsilon_S \cdot E \end{cases} \quad (3)$$

Where  $T$ ,  $S$ ,  $E$ , and  $D$  are the stress, strain, electric, and dielectric displacement fields, whereas  $c_E$ ,  $e$ , and  $\epsilon_S$  are the mechanical stiffness, the piezoelectric, and the permittivity

coefficient tensor, respectively. The mechanical stress free boundary condition requires that stresses normal to the six faces are equal to zero:

$$\int_{-a_2}^{a_2} \int_{-a_3}^{a_3} T_1(a_1) dx_3 dx_2 = 0 = \int_{-a_2}^{a_2} \int_{-a_3}^{a_3} c_E \cdot S(a_1) dx_3 dx_2 + (e_{k,1})^t \cdot \int_{-a_2}^{a_2} \int_{-a_3}^{a_3} \begin{pmatrix} E_1(a_1) \\ E_2(a_1) \\ E_3(a_1) \end{pmatrix} dx_3 dx_2 \quad (4)$$

The sample's dimension is  $-a_i$  to  $a_i$  along  $x_i$ . The leakage current along the surfaces is assumed to be negligible. Also, the voltage between two opposite faces is considered to be zero, except between the two electrodes, where the voltage is equal to  $V$ . We therefore find from Equation 3 that

$$\int_{-a_1}^{a_1} \int_{-a_2}^{a_2} \int_{-a_3}^{a_3} \begin{pmatrix} D_1 \\ D_2 \\ D_3 \end{pmatrix} dx_1 dx_2 dx_3 = e \cdot \int_{-a_1}^{a_1} \int_{-a_2}^{a_2} \int_{-a_3}^{a_3} S dx_1 dx_2 dx_3 + \epsilon_S \cdot \int_{-a_1}^{a_1} \int_{-a_2}^{a_2} \int_{-a_3}^{a_3} \begin{pmatrix} E_1 \\ E_2 \\ E_3 \end{pmatrix} dx_1 dx_2 dx_3 \quad (5)$$

Integrating the dielectric displacement over the volume of the sample leads to the free electric charge  $Q$  (equal to the first term in Equation 5), whereas integrating the electric field gives the voltage  $V$  (equal to the last term in Equation 5). The electrochemical impedance  $Z$  is then obtained by taking the ratio of the voltage over the current  $I$  for a sinusoidal excitation with frequency  $f = \omega / 2\pi$ ,

$$Z(\omega) = \frac{V}{I} = \frac{V}{-j\omega Q} = Z_0(\cos \phi + j \sin \phi), \quad (6)$$

where  $j$  is the imaginary number and  $\phi$  is the angular phase shift in radians. In the interest of brevity, the fully expanded expression for Equation 6 is not provided; fully expanded, the expression covers tens of pages, as lithium niobate is in the highly asymmetric 3m crystal class. However, the reader may readily expand the expression themselves by employing Matlab, Mathematica, Maple, or a similar program. Since this model is general in nature, the solution to the 3m crystal class permits us to study monocrystalline lithium niobate [20,21]. A 10 mm x 10 mm x 0.5 mm Y-cut sample of a congruent-melt-grown single crystal of lithium niobate was used, although any known, arbitrary geometry could have been employed. The density of the material was estimated as 4.64 g/cm<sup>3</sup> [22]. A 100 nm thick platinum electrode on a titanium dioxide adhesion layer was sputtered onto both sides of the crystal to produce a parallel plate metal-oxide-metal (MOM) capacitor structure. The lithium niobate sample was placed on a hot plate placed in a quartz tube to avoid thermal perturbations. An E4990A Keysight impedance analyzer was used to measure the electrochemical impedance spectrum of the sample using platinum contacts.

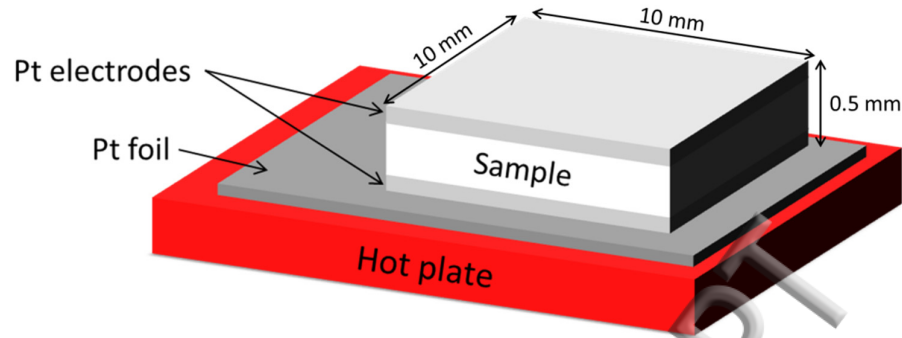


Fig. 1. Experimental setup for high temperature measurements.

The sample was heated in steps of 100 °C up to 500 °C and then in steps of 50 °C up to 750 °C, at a rate of 50 degrees per minute. Each step was maintained for at least fifteen minutes. For samples of the chosen geometry, the first non-negligible resonance is a radial mechanical vibrational resonance at  $f = 282$  kHz, whereas the thickness mode appears around 6.3 MHz. The resonant frequencies are a function of the sample geometry, density, and material parameters. Since the sample geometry and density are readily known, it is therefore possible to directly extract all relevant material parameters from a single electrochemical impedance spectrum. Since the model fits multiple resonances over the entire spectrum simultaneously, a wider frequency range covering a large number of resonance peaks provides more precise results. However, in order to have the best compromise between measurement speed and precision, the electrochemical impedance was measured from 250 kHz to 7 MHz, with values normalized to the electrode area. The analytical model was simultaneously fitted to the entire range of the measured impedance spectrum using a cost function (Equation 7). Performing a best-fit regression of the analytical model (Equation 6) to the entire measured electrochemical impedance spectrum using the cost function (Equation 7) enables the entirety of the material parameters to be extracted simultaneously in a global approach using all predicted resonant frequencies at once. The precision of determining the material parameters is exceptional, as all data points of the spectrum (in our case, over 8000 points for a single measured spectrum containing multiple resonances) were taken into account.

$$\text{Cost} = \sum \left( (\log(|Z_{\text{model}}|) - \log(|Z_{\text{meas}}|))^2 + (\phi_{\text{model}} - \phi_{\text{meas}})^2 \right) \quad (7)$$

### 3. Results and Discussion

Figure 2 shows the model fitted to a representative experimental measurement performed at room temperature. Despite numerous harmonics and a large range, the model accurately predicts the experimental observations over the entire range measured. Numerical simulations show that, for our sample geometry, the two resonances at 282 kHz and 360 kHz correspond to radial mechanical vibrational resonance modes. The first mode has two radial waves out of phase, whereas the second mode has radial waves in-phase. The high frequency resonances at 3.6 MHz and 6.3 MHz are the shear mode and the thickness mode, respectively. All these principal resonances, which correspond to pure modes, are well described by the analytical

model. The diversity of the different modes with the Y-cut orientation gives, simultaneously, a good characterization of all electromechanical material property coefficients [23,24]. At high frequencies, minor higher order harmonics appear as small peaks and can be easily mistaken for noise; although the analytical model does not predict all of these higher order harmonics, the fitting is stable and provides results consistent with the literature, as shown in table 1.

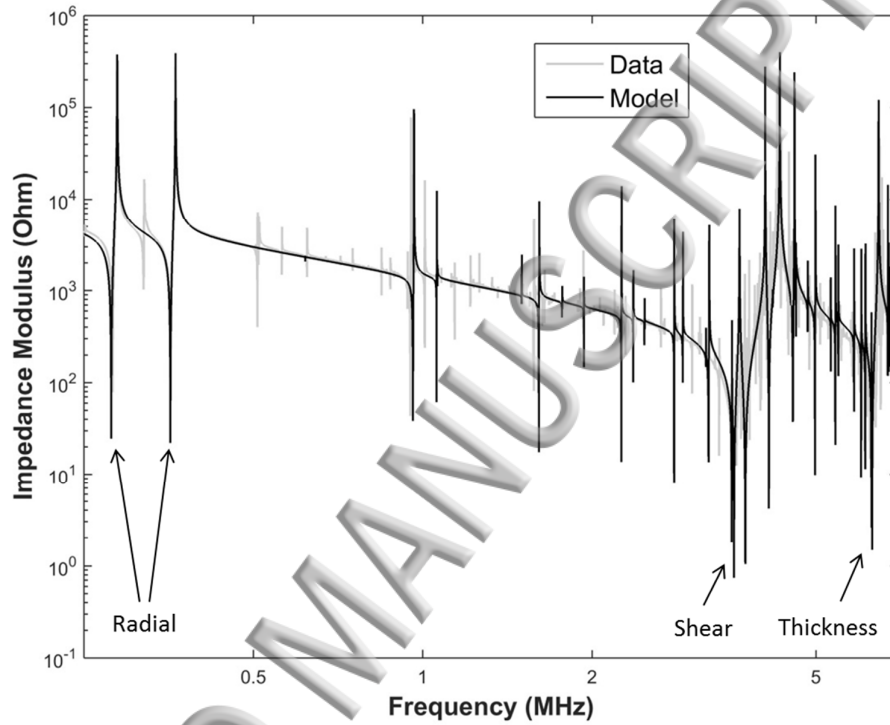


Fig.2: Electrochemical impedance modulus spectrum of LiNbO<sub>3</sub> at 23 °C.

Table 1. Material properties of LiNbO<sub>3</sub> as a function of temperature

Temperature (°C)	C <sub>11</sub> (GPa)	C <sub>12</sub> (GPa)	C <sub>13</sub> (GPa)	C <sub>14</sub> (GPa)	C <sub>33</sub> (GPa)	C <sub>44</sub> (GPa)	e <sub>15</sub> (C/m <sup>2</sup> )	e <sub>22</sub> (C/m <sup>2</sup> )	ε <sub>1</sub> (1)
Literature reference at 25°C [22]	203	57.5	75.2	8.5	242.4	59.5	3.76	2.43	44.3
Measured values at 23°C	203	59.9	72.5	7.97	236	58.7	3.89	2.46	47.8
100	201	61.5	71.1	7.80	236	57.9	3.88	2.45	50.0

200	197	61.4	71.5	7.58	234	56.5	3.96	2.51	52.0
300	194	64.6	70.3	6.73	233	56.6	4.06	2.51	54.9
400	191	65.4	71.5	6.26	232	55.5	4.15	2.49	58.2
500	187	66.6	71.1	6.25	231	54.0	4.21	2.62	63.8
550	186	66.1	69.0	6.64	229	53.4	4.27	2.54	65.3
600	185	66.5	68.7	5.84	227	53.5	4.32	2.51	68.1
650	184	66.2	67.2	7.04	226	53.0	4.34	2.61	74.7
700	182	62.9	67.5	6.69	224	52.8	4.02	2.56	76.9
750	179	67.5	61.8	7.12	224	52.8	4.21	2.55	83

The material coefficients provided in Table 1 were extracted from the electrochemical impedance spectrum measured at the given temperature. A best-fit regression analysis of the analytical model described by equation 5 to the entire spectrum, measured from 250 kHz to 7 MHz, simultaneously takes into account all predicted resonance peaks. In this global approach, the coefficients are extracted from all predicted resonance modes simultaneously over a wide frequency range. Therefore, the accuracy of each coefficient depends on its degree of involvement in the resonances measured. Thus, the electrochemical spectrum measurement was design to catch the radial, shear and thickness mode together in order to provide a good accuracy on  $C_{11}$  and  $C_{33}$  and  $e_{22}$  (radial),  $C_{44}$  and  $e_{15}$  (shear) and  $C_{11}$  and  $e_{22}$  (thickness). The accuracy of coupling coefficient such as  $C_{12}$  and  $C_{13}$  is lower due to the lower sensitivity of the model to these coefficients.

The effect of temperature on selected material parameters is shown in Figure 3. The other coefficients follow the same trends. As expected, the mechanical stiffness coefficients decrease with temperature, whereas the dielectric permittivity increases with temperature. This is consistent with the understanding that the material softens with temperature, thereby reducing the phonon velocity. On the other hand, the thermal expansion of the crystalline structure allows for a larger dielectric displacement, and thus a higher permittivity [25]. Also, since the piezoelectric coefficients are a function of crystallographic symmetry, they will not be affected an isotropic thermal dilatation [26]; however, phase changes or anisotropic strains would have an impact.

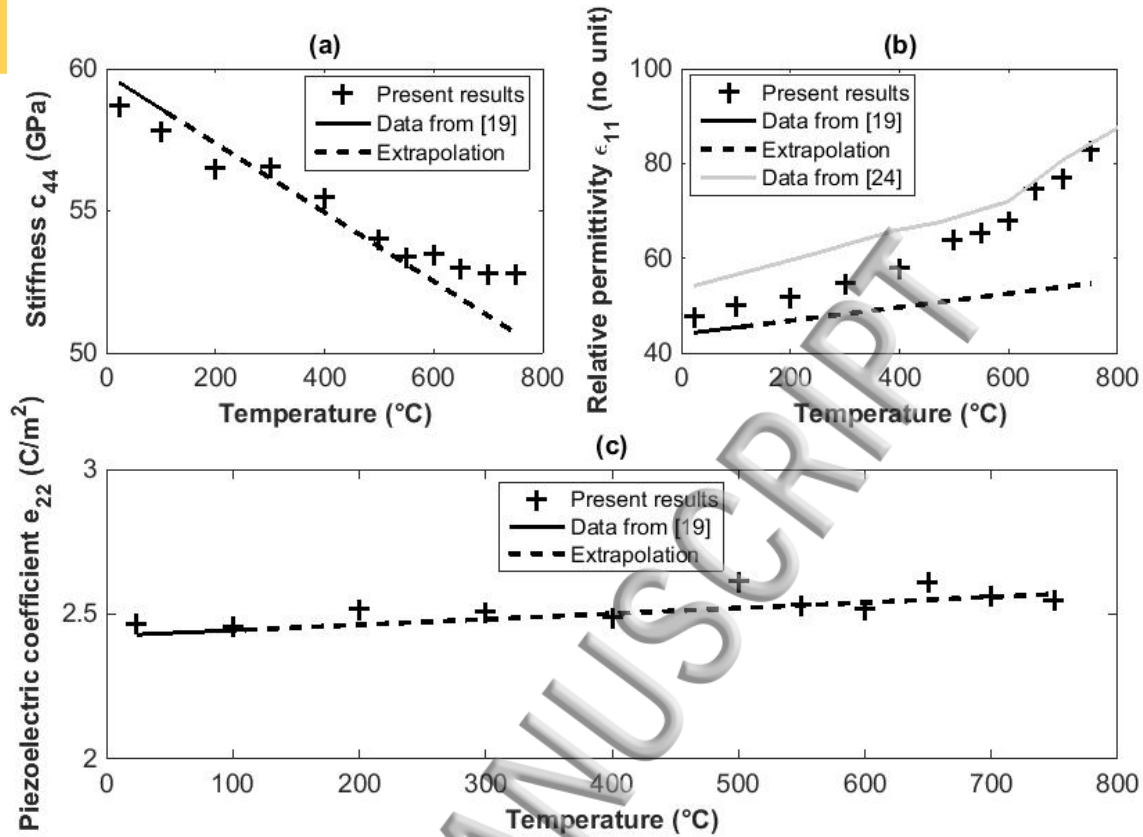


Fig 3. (a) Stiffness coefficient  $C_{44}$  (GPa); (b) Relative permittivity  $\epsilon_1$  (1); and (c) Piezoelectric coefficient  $e_{22}$  (C/m<sup>2</sup>), as a function of temperature. Values from Smith and Welsh [22] with its extrapolation for temperatures above 110 °C and values from Poplavko [27] are also plotted for reference.

The coefficients extracted by the model and their temperature dependence are comparable to the values taken directly from Smith and Welsh [22]. The relative permittivity follow an exponential law as a function of temperature [25]. Then, the linear extrapolation is unsuitable at high temperature. A comparison with experimental data from Poplavko shows that the extracted values are compatible with previous measurements. However, the model used in this article takes into account more parameters than previous models. Thus, it is not surprising to have a slight discrepancy with the previous literature that used simpler models, as these additional parameters improve the reliability of the values extracted. For example, some coefficients not considered in traditional models include the secondary stiffness coefficients like  $c_{12}$ , even though they affect the main resonances and then impact the parameters extracted. Since the present model considers more coefficients and simultaneously fits the entire electrochemical impedance spectrum (as opposed to traditional models that only fit a single resonance at a time), it is harder to have a good fit at every frequency but the values deduced are more accurate over the entire studied frequency range.

The few previous studies on the piezoelectric behavior of lithium niobate in the kHz region have suggested that ionic conductivity can deteriorate the piezoelectric performance of this material at high temperatures, although this hypothesis has not yet been confirmed in the literature [28,29]. In order to further explore this hypothesis, we compare the electrochemical impedance spectrum of higher frequencies (several MHz) to lower frequencies (100s of kHz); ionic conductivity is known to be less of a concern at higher frequencies, since ions typically have a higher effective mass than electrons. Figure 4 shows a typical electrochemical impedance spectrum that at first appears to be affected by ionic (or vacancy) conductivity (measured at 23 °C). Indeed, equivalent circuit analysis typically represents such conductivity as a resistor in parallel with the piezoelectric capacitor. On an electrochemical impedance spectrum, the impedance modulus will be limited by this equivalent resistance. In Figure 4, we find that, for the spectrum measured at 750 °C, values above about 2000  $\Omega$  collapse, apparently consistent with an equivalent resistance of about 2000  $\Omega$ .

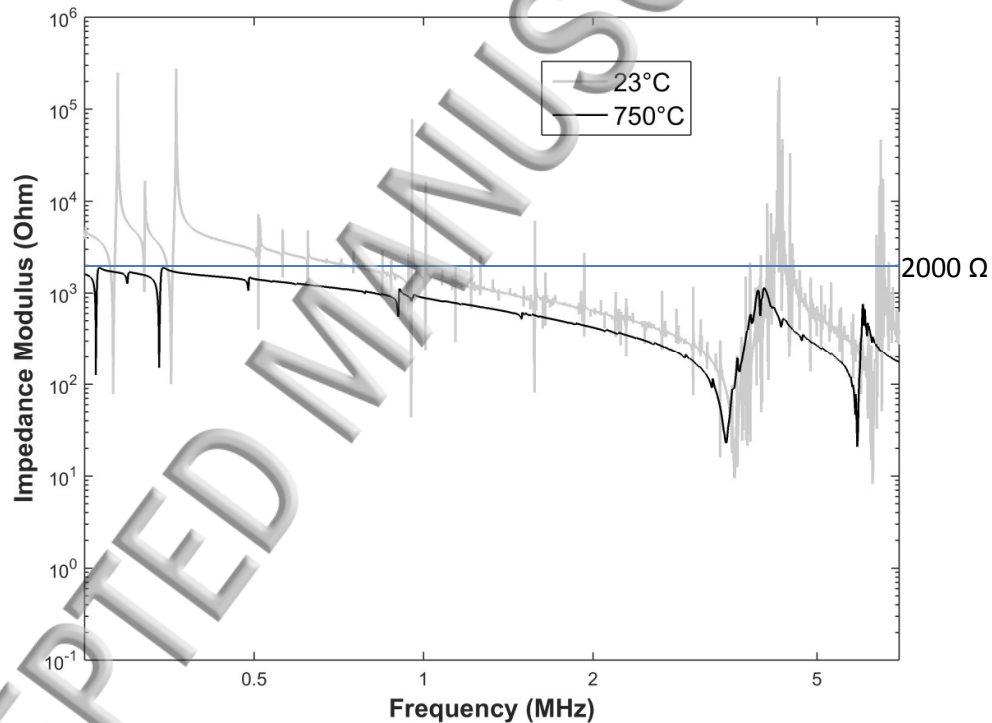


Fig. 4: Electrochemical impedance spectrum of  $\text{LiNbO}_3$  measured at 23 °C and 750 °C.

Nevertheless, more careful observation shows that the impedance is limited to about 2000  $\Omega$  across the entire frequency range measured. This is inconsistent with ionic conductivity: ions and vacancies are large point defects that will play a larger role at lower frequencies (kHz), where their mobility is sufficient to follow the electric field. We therefore suspect a possible measurement artifact based on the thermoelectric effect, which would be expected to have the same apparent effect as ionic conductivity on the impedance spectrum, except across a much

wider frequency range: thermoelectric phenomena involve electrons, which are more mobile than ions or vacancies; electrons can more readily follow the electric field, even at higher frequencies (MHz). Despite this measurement artifact observed at high temperatures, the resonances are still clearly visible and piezoelectric coefficients were readily extracted (Figure 3) – there is therefore no degradation of the piezoelectric behavior across the frequency spectrum measured.

In addition to characterizing the material properties of lithium niobate for elevated temperatures up to 750 °C, we can therefore rule out ionic or vacancy conductivity as a degradation mechanism affecting piezoelectric behavior at high frequencies. While further work is necessary to characterize the possible efficiency of a high temperature piezoelectric lithium niobate device, our findings suggest that lithium niobate is a suitable candidate for high frequency piezoelectric applications up to 750 °C, although care should be taken to reduce thermal gradients across the piezoelectric device.

#### 4. Conclusions

We find that that lithium niobate is a promising candidate for high temperature piezoelectric applications up to at least 750 °C, including at high frequencies up to the MHz region. A possible thermoelectric effect can complicate the measurement of material properties at high temperature, and likely explains the “ionic conductivity” previous authors believed to have observed. We conclude that such ionic or vacancy conductivity is not a significant degradation mechanism in single crystal LiNbO<sub>3</sub> below 750 °C, since such a mechanism is incompatible with the high frequency behavior observed.

#### Acknowledgements

The authors wish to thank the Natural Sciences and Engineering Research Council of Canada (NSERC) Discovery Grant program for financial support

#### References

- [1] R. Wang, S.A. Bhave, K. Bhattacharjee, High  $kt^2xQ$ , multi-frequency lithium niobate resonators, Proc. IEEE 26th Int. MEMS Conf. (2013) 165–168.
- [2] L. Shi, G. Piazza, Lithium Niobate on Silicon Dioxide Suspended Membranes: a Technology Platform for Engineering the Temperature Coefficient of Frequency of High Electromechanical Coupling Resonators, J. Microelectromechanical Syst. 23 (2013) 1318–1329.
- [3] M.R.H. Sarker, et al., A Lithium Niobate High-Temperature Sensor for Energy System Applications., IEEE Sens. J. 16 (2016) 5883–5888.

- [4] R. Kažys, a Voleišis, B. Voleišienė, High temperature ultrasonic transducers : review, *Ultrasound*. 63 (2008) 7–17. [http://www.ktu.lt/ultra/journal/pdf\\_63\\_2/63-2008-No.2\\_01-Kazys.pdf](http://www.ktu.lt/ultra/journal/pdf_63_2/63-2008-No.2_01-Kazys.pdf).
- [5] K. Shinekumar, S. Dutta, High-Temperature Piezoelectrics with Large Piezoelectric Coefficients, *J. Electron. Mater.* 44 (2014) 613–622. doi:10.1007/s11664-014-3534-2.
- [6] A. Baba, C.T. Searfass, B.R. Tittmann, High temperature ultrasonic transducer up to 1000°C using lithium niobate single crystal, *Appl. Phys. Lett.* 97 (2010) 1–4. doi:10.1063/1.3524192.
- [7] A. Weidenfelder, J. Shi, P. Fielitz, G. Borchardt, K.D. Becker, H. Fritze, Electrical and electromechanical properties of stoichiometric lithium niobate at high-temperatures, *Solid State Ionics*. 225 (2012) 26–29. doi:10.1016/j.ssi.2012.02.026.
- [8] D. Damjanovic, Materials for high temperature piezoelectric transducers, *Curr. Opin. Solid State Mater. Sci.* 3 (1998) 469–473. doi:10.1016/S1359-0286(98)80009-0.
- [9] D. Parks, S. Zhang, B. Tittmann, High-temperature (> 500°C) ultrasonic transducers: an experimental comparison among three candidate piezoelectric materials, *IEEE Trans. Ultrason. Ferroelectr. Freq. Control.* 60 (2013) 1010–1015. [http://ieeexplore.ieee.org/xpls/abs\\_all.jsp?arnumber=6512839](http://ieeexplore.ieee.org/xpls/abs_all.jsp?arnumber=6512839).
- [10] R.C. Turner, P.A. Fuierer, R.E. Newnham, T.R. Shrout, Materials for high temperature acoustic and vibration sensors: A review, *Appl. Acoust.* 41 (1994) 299–324. doi:10.1016/0003-682X(94)90091-4.
- [11] S. Zhang, F. Yu, Piezoelectric materials for high temperature sensors, *J. Am. Ceram. Soc.* 94 (2011) 3153–3170. doi:10.1111/j.1551-2916.2011.04792.x.
- [12] N. Standard, IEEE Standard on Piezoelectricity, East. (1988) 74. doi:10.1109/IEEESTD.1988.79638.
- [13] S. Zhu, B. Jiang, W. Cao, Characterization of piezoelectric materials using ultrasonic and resonant techniques, *Proc. SPIE*. 3341 (1998) 154–162. doi:10.1117/12.307996.
- [14] W. Cao, S. Zhu, B. Jiang, I. Introduction, Analysis of shear modes in a piezoelectric vibrator, *J. Appl. Phys.* 83 (1998) 4415–4420. doi:10.1063/1.367233.
- [15] A.W. Warner, M. Onoe, G.A. Coquin, Determination of Elastic and Piezoelectric Constants for Crystals in Class (3m), *J. Acoust. Soc. Am.* 42 (1967) 1223. doi:10.1121/1.1910709.
- [16] H. de Castilla, P. Belanger, R.J. Zednik, General dynamic analytical model of piezoelectric materials, *Submitt. to Nature Scientific Reports*. (n.d.).
- [17] M. Brissaud, Characterization of Piezoceramics, *IEEE Trans. Ultrason. Ferroelectr. Freq. Control.* 38 (1991) 603–617. doi:10.1109/58.108859.
- [18] M. Brissaud, Three-dimensional modeling of piezoelectric materials, *IEEE Trans. Ultrason. Ferroelectr. Freq. Control.* 57 (2010) 2051–2065. doi:10.1109/TUFFC.2010.1653.
- [19] H.A. Kunkel, S. Locke, B. Pikeroen, Finite-Element Analysis of Vibrational Modes in

- Piezoelectric Ceramic Disks, IEEE Trans. Ultrason. Ferroelectr. Freq. Control. 37 (1990) 316–328. doi:10.1109/58.56492.
- [20] G. Gautschi, Piezoelectric Sensorics, 2002. doi:10.1007/978-3-662-04732-3.
- [21] K.-K. Wong, Properties of lithium niobate, IET, 2002.
- [22] R.T. Smith, F.S. Welsh, Temperature Dependence of the Elastic, Piezoelectric, and Dielectric Constants of Lithium Tantalate and Lithium Niobate, J. Appl. Phys. 42 (1971) 2219. doi:10.1063/1.1660528.
- [23] J.F. Nye, Physical properties of crystals: their representation by tensors and matrices, Oxford university press, 1985.
- [24] B. Jaffe, W.R. Cook, H.L. Jaffe, Piezoelectric ceramics, Academic Press, 1971.
- [25] B.S. Umarov, J.F. Vetelino, N.S. Abdullaev, A.A. Anikiev, Temperature dependence of the dielectric constant and I.R. reflection spectrum of LiNbO<sub>3</sub> by Raman scattering, Solid State Commun. 36 (1980) 465–468. doi:10.1016/0038-1098(80)90935-7.
- [26] D. Das, T. Jacobs, L.J. Barbour, Exceptionally large positive and negative anisotropic thermal expansion of an organic crystalline material, Nat. Mater. 9 (2010) 36–39. doi:10.1038/nmat2583.
- [27] Y.M. Poplavko, V.V. Meriakri, V.N. Aleshechkin, V.G. Tskalov, E.F. Ushatkin, A.S. Knyazev, Dielectric spectrum of lithium niobate, Fiz. Tverd. Tela. 15 (1973) 1473–1476.
- [28] G. Bergman, The electrical conductivity of LiNbO<sub>3</sub>, Solid State Commun. 6 (1968) 77–79. doi:10.1016/0038-1098(68)90004-5.
- [29] P. Jorgensen, R. Bartlett, High temperature transport processes in lithium niobate, J. Phys. Chem. Solids. 30 (1969) 2639–2648. <http://www.sciencedirect.com/science/article/pii/0022369769900377>.

